Stem Cell Reports
Article

ISSCR

OPEN ACCESS

In Vitro Generation of Vascular Wall-Resident Multipotent Stem Cells of Mesenchymal Nature from Murine Induced Pluripotent Stem Cells

Jennifer Steens,[1,4] Melanie Zuk,[2,4] Mohamed Benchellal,[1] Lea Bornemann,[1] Nadine Teichweyde,[2] Julia Hess,[3] Kristian Unger,[3] André Görgens,[2] Hannes Klump,[2] and Diana Klein[1,*]

[1]Institute of Cell Biology (Cancer Research), University Hospital Essen, Medical Faculty, University of Duisburg-Essen, 45122 Essen, Germany
[2]Institute for Transfusion Medicine, University Hospital Essen, University of Duisburg-Essen, 45122 Essen, Germany
[3]Research Unit Radiation Cytogenetics, Helmholtz Zentrum München, German Research Center for Environmental Health GmbH, 85764 Neuherberg, Germany
[4]Co-first author
*Correspondence: diana.klein@uk-essen.de
http://dx.doi.org/10.1016/j.stemcr.2017.03.001

SUMMARY

The vascular wall (VW) serves as a niche for mesenchymal stem cells (MSCs). In general, tissue-specific stem cells differentiate mainly to the tissue type from which they derive, indicating that there is a certain code or priming within the cells as determined by the tissue of origin. Here we report the in vitro generation of VW-typical MSCs from induced pluripotent stem cells (iPSCs), based on a VW-MSC-specific gene code. Using a lentiviral vector expressing the so-called Yamanaka factors, we reprogrammed tail dermal fibroblasts from transgenic mice containing the GFP gene integrated into the *Nestin*-locus (NEST-iPSCs) to facilitate lineage tracing after subsequent MSC differentiation. A lentiviral vector expressing a small set of recently identified human VW-MSC-specific *HOX* genes then induced MSC differentiation. This direct programming approach successfully mediated the generation of VW-typical MSCs with classical MSC characteristics, both in vitro and in vivo.

INTRODUCTION

A frequently used source of mesenchymal stem cells (MSCs) is bone marrow. Such MSCs are commonly used as immune-suppressants for the treatment of steroid-refractory graft-versus-host disease after transplantation of hematopoietic stem cell-containing preparations, as MSCs elicit a weak allogeneic immune response when delivered into a non-identical, non-matched recipient (Nauta and Fibbe, 2007; Pittenger et al., 1999; Schu et al., 2012). However, bone marrow extraction is a highly invasive procedure and only 0.01% to 0.001% of the collected cells are MSCs. Therefore, more easily accessible sources of MSCs are needed.

In contrast to bone marrow, MSCs can be easily harvested from various other adult human tissues, including cord blood, placenta, peripheral blood, adipose tissue, and the vessel wall (Gotherstrom et al., 2005; Jin et al., 2013; Klein et al., 2011; Zhu et al., 2014). However, variations of the quality of obtained donor cells and tissue sources, as well as subsequent cell culture, have caused numerous inconsistencies in the reported in vivo effectiveness of MSCs (Galipeau, 2013; Kimbrel et al., 2014; Tyndall, 2014; Wagner and Ho, 2007). Although these rare post-natal stem cells can be rapidly expanded in vitro to obtain the numbers necessary for therapeutic use, vigorous ex vivo expansion can result in replicative senescence and lead to a decline of their plasticity (e.g., alterations in cell-cycle or apoptosis pattern while maintaining the normal karyotype and phenotypic characteristics) and in vivo potency over time (Ho et al., 2013; Kyriakou et al., 2008; Liu et al., 2012; Miura et al., 2006; Rombouts and Ploemacher, 2003). Finally, tissue stem cells may have accumulated many DNA abnormalities (caused by sunlight, toxins, and errors during DNA replication) during a lifetime (Janzen et al., 2006; Mimeault and Batra, 2009). These potential drawbacks may limit their usefulness.

An alternative method to circumvent many of these issues is to obtain MSCs by their generation from induced pluripotent stem cells (iPSCs) in vitro. Use of allogeneic standardized, validated, and officially approved iPSC banks would allow the generation of "off-the-shelf" MSCs with comparable properties and in large quantities (Jung et al., 2012; Kimbrel et al., 2014; Okano et al., 2013; Lindvall and Kokaia, 2010). The classical method for differentiating iPSCs toward MSCs is the use of medium that contains a high serum concentration or MSC-typical growth factors such as basic fibroblast growth factor after dissociation of embryoid bodies (Frobel et al., 2014; Jung et al., 2012; Liu et al., 2012).

We have previously shown that vascular wall-derived MSCs (VW-MSCs) particularly were more potent than bone marrow-derived MSCs in protecting lung endothelial cells from the adverse late effects of radiotherapy (Klein et al., 2016a, 2016b). These findings support the assumption that tissue-specific stem cells support the tissue type from which they originate, which is a central advantage for the use of VW-MSCs for the protection and curative treatment of vascular structures (Ergun et al., 2011; Klein, 2016; Klein et al., 2016a). Previous reports have already

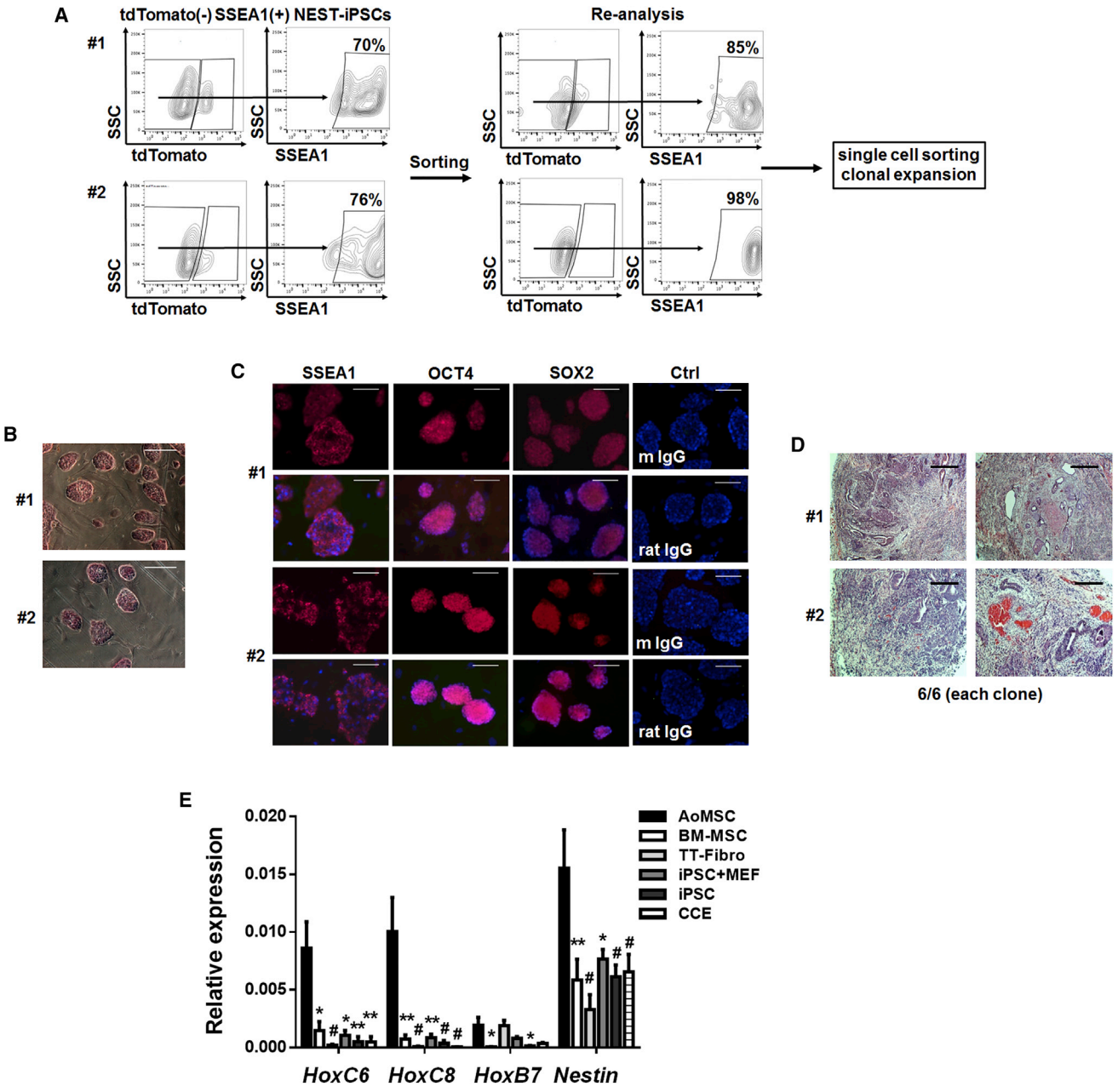

Figure 1. Pluripotency Profiling of Generated NEST-iPSCs

(A) Reprogrammed dermal tail-tip fibroblasts derived from transgenic NEST-GFP mice (bona fide iPSCs) were analyzed by flow cytometry. dtTomato^{-}SSEA1^{+} were sorted as single cells, clonally expanded, and established as independent cell lines. Representative contour plots from two fibroblast isolates (#1, #2) from n = 3 independent experiments are shown.

(B) Expression of alkaline phosphatase in clonally expanded iPSCs cultured on mouse embryonic fibroblasts (MEFs) was detected by alkaline phosphatase activity staining (red). Representative photographs for two different clones (#1, #2) from n = 6 independent experiments are shown. Scale bars, 100 μm.

(C) Immunofluorescence stainings were performed for surface (SSEA1) and nuclear (OCT4, SOX2) antigens showing expression (red) of pluripotency-associated proteins in two dtTomato^{-} NEST-iPSC clones (#1, #2) from n = 4 independent experiments. Nuclei were counterstained using DAPI. Scale bars, 100 μm.

(D) H&E-stained histology was performed of teratomas formed by two different clones (#1, #2) 4 weeks after subcutaneous transplantation (n = 6 mice per clone, n = 12 mice in total). Scale bars, 200 μm.

(legend continued on next page)

demonstrated that bone marrow-derived MSCs were less effective for MSC therapy than other stem cell sources, e.g., when compared with adipose tissue-derived or fetal MSCs, respectively (Montesinos et al., 2009; Prasanna et al., 2010; Ribeiro et al., 2013; Wang et al., 2014; Wegmeyer et al., 2013; Zhang et al., 2009).

The tissue-specific homing and activities of MSCs that have been cultured in vitro prior to transfusion are likely based on an underlying transcriptional code caused by epigenetic memory allowing them to home back to the tissue from which they originally were derived (Frobel et al., 2014). We have previously identified certain homeodomain-containing master regulators (homeotic selector [*HOX*] gene family members) which are selectively expressed in VW-MSCs (Klein et al., 2013). Comparison of the expression patterns of 39 *HOX* genes in these cells with terminally differentiated endothelial cells, smooth muscle cells (SMCs), and undifferentiated embryonic stem cells revealed that the *HOX* genes *HOXB7*, *HOXC6*, and *HOXC8* were specifically upregulated in VW-MSCs (Klein et al., 2013).

In this work, we now demonstrate that iPSCs can be directly programmed toward mouse VW-typical multipotent stem cells of mesenchymal nature by ectopic lentiviral expression of the VW-MSC-specific *HOX* code encompassing *HOXB7*, *HOXC6*, and *HOXC8*, which we had previously defined. Provided that this approach can be translated to human cells, it may be particularly well suited for the treatment of diseases associated with vascular damage and remodeling, such as hypertension, ischemic diseases, congenital vascular lesions (aneurysms, fibromuscular hyperplasia, stenosis in collaterals), shear stress, or irradiation (Gibbons and Dzau, 1994; Korshunov et al., 2007; Renna et al., 2013).

RESULTS

Derivation and Characterization of *HOX*-Transduced and Control NEST-iPSCs

We reprogrammed primary dermal tail-tip fibroblasts from a transgenic mouse in which the gene encoding GFP is expressed under the regulatory control of the *Nestin* promoter (NEST-GFP). Transduction of fibroblasts was performed with a lentiviral vector co-expressing the four Yamanaka factor genes (*OCT4*, *KLF4*, *SOX2*, and *MYC*) together with the coding sequence of the red fluorescent tdTomato protein. The reprogramming efficiencies (i.e., the number of isolated colonies per transduced cells) were similar for fibroblasts derived from different NEST-GFP donor mice, ranging from 1% to 3% (Table S1). For quality and potency characterization of the generated bona fide iPSCs, we isolated cells that had silenced the reprogramming vector (dtTomato$^-$) and expressed SSEA1$^+$ by flow-cytometric cell sorting, subsequently expanded NEST-iPSC clones (12 in total), and established those as independent cell lines. Quality testing included flow-cytometric analysis of SSEA1 expression, alkaline phosphatase staining, and immunofluorescence staining of pluripotency-associated markers (SSEA1, SOX2, and OCT4) (Figure 1). Alkaline phosphatase was active in all isolated dtTomato$^-$SSEA1$^+$ NEST-iPSC clones (Figures 1A and 1B). Expression of the nuclear proteins OCT4 and SOX2 and the cell-surface antigen SSEA1 was demonstrated by immunofluorescence (Figure 1C). As the most stringent test for pluripotency of iPSCs, teratoma assays were performed. Mice were injected with reprogrammed cells of two selected clones. Tumors formed within 4–6 weeks with 100% efficiency (6/6 per clone). Histomorphological analysis after H&E staining revealed that these tumors contained derivatives of all three germ layers (Figures 1D and S1). Conclusively, all tests applied for quality and potency indicated that the newly generated mouse NEST-iPSCs were pluripotent and fully reprogrammed.

We then compared the expression of the three selected VW-MSC-specific, endogenous *HOX* candidate genes (*HoxB7*, *HoxC6*, and *HoxC8*), as well as of the MSC marker *Nestin* in the reprogrammed NEST-iPSCs, mouse VW-derived (aorta) MSCs (AoMSCs), bone marrow-derived MSCs (BM-MSCs), tail-tip dermal fibroblasts (TT-Fibro), and pluripotent mouse embryonic stem cells derived from the 129/Sv/Ev strain (line CCE) (Figure 1E). Expression of all three *HOX* genes was exclusively detected in cells from adult tissue. In AoMSCs, significantly higher expression levels of *HoxC6*, *HoxC8*, *HoxB7*, and *Nestin* were detected than in the iPSCs, CCE cells, or BM-MSCs.

Ectopic Expression of *HOXB7*, *HOXC6*, and *HOXC8* Enforces the Generation of NEST$^+$ Cells during iPSC Differentiation

To test whether VW-specific MSCs can specifically be obtained by forward programming in vitro, we transduced

(E) Differential expressions of the three selected *HOX* candidates and *Nest* were analyzed by qRT-PCR in vascular wall-derived (aortic) MSCs (AoMSCs) compared with bone marrow-derived MSCs (BM-MSCs), isolated tail-tip fibroblasts (TT-Fibro) from NEST-GFP transgenic mice, generated NEST-iPSCs cultured on MEFs (iPSC + MEF), or cultured free of feeder-layer on gelatine (iPSCs), and to the mouse embryonic stem cells CCE. Shown are mean values ± SEM from at least n = 3 independent samples per group each measured in duplicates (biological replicates: AoMSC, n = 8–10; BM-MSC, n = 3; TT-Fibro, n = 5; iPSC + MEF, n = 3; iPSC, n = 5–6; CCE, n = 5); p values calculated by two-way ANOVA followed by post hoc Bonferroni test. *$p \leq 0.05$, **$p \leq 0.01$, $^{\#}p \leq 0.005$.
See also Figure S1.

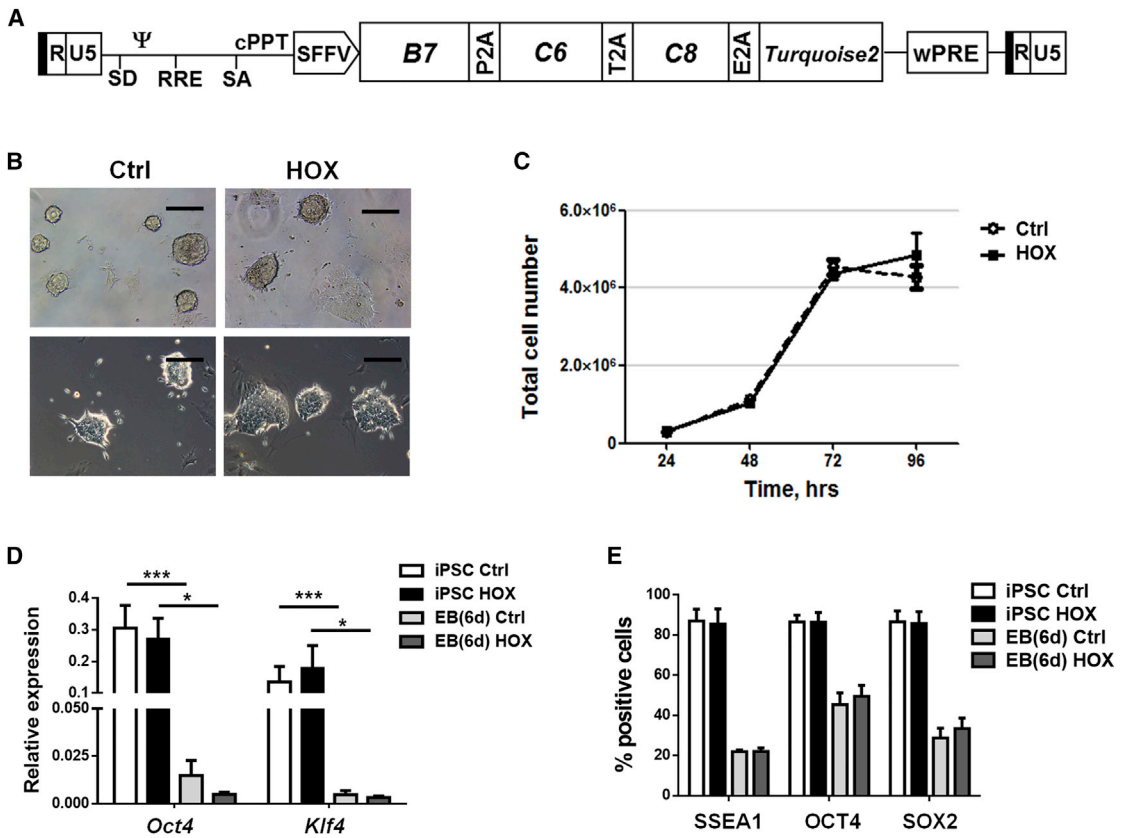

Figure 2. Derivation and Characterization of *HOX*-Transduced and Control NEST-iPSCs

(A) Scheme of the lentiviral SIN vector co-expressing the coding sequences of *HOXB7*, *HOXC6*, and *HOXC8* separated by *2A esterase* elements together with the gene encoding the reporter TURQUOISE2 fluorescent protein.

(B) Typical cell morphology was analyzed by phase-contrast microcopy. Representative photographs of n = 3 independent experiments are shown. Scale bars, 150 μm.

(C) Cell proliferation was analyzed by cell counting the *HOX*- and control-transduced NEST-iPSC 48 hr after transduction at the indicated time points after plating (200,000 cells per well). Data are shown as means ± SEM of n = 3 independent experiments.

(D) qRT-PCR quantifications of the pluripotent markers *Pou5f1/Oct4* and *Klf4* were performed in respective iPSCs 2 days after transduction and in aggregated EBs after an additional 2 days (biological replicates: n = 6–9 per group and gene); p values calculated by one-way ANOVA followed by post hoc Bonferroni test.*$p \leq 0.05$, ***$p \leq 0.005$.

(E) Single-cell suspensions of control and *HOX*-transduced NEST-iPSCs and of aggregated EBs were analyzed by fluorescence-activated cell sorting (FACS) with indicated antibodies. Data are presented as mean ± SEM from at least n = 3 independent experiments (biological replicates: n = 6–8 for each epitope and group).

feeder-free cultured NEST-iPSCs with a self-inactivating (SIN) lentiviral vector co-expressing the coding sequences of *HOXB7*, *HOXC6*, and *HOXC8* separated by *2A esterase* elements together with the gene encoding mTURQUOISE2 (mCyan-derived) fluorescent protein (Figure 2A). The process of transduction as such did not alter cell morphology (Figure 2B) or cell proliferation of the iPSCs (Figure 2C). The undifferentiated cells still expressed the endogenous pluripotency-associated genes *Pou5f1* (encoding *Oct4*) and *Klf4* as evaluated by qRT-PCR (Figure 2D) and flow-cytometric analysis of SSEA1, OCT4, and SOX2 expression (Figure 2E). Their ability to differentiate was also not altered by the ectopic expression of these three *HOX* genes as evaluated by embryoid body (EB) formation and with significantly decreased expression of pluripotency-associated genes. Again, teratoma assays were performed in immunodeficient NMRI mice with the transduced NEST-iPSCs. Tumors again formed with 100% efficiency. Histomorphological analysis revealed that all tumors contained derivatives of all three germ layers (Figure 3), again proving the pluripotency of the obtained NEST-iPSCs, irrespective of ectopic *HOX* expression.

Expression of the endogenous and ectopic HOX proteins was confirmed by western blotting (Figure 4A) and

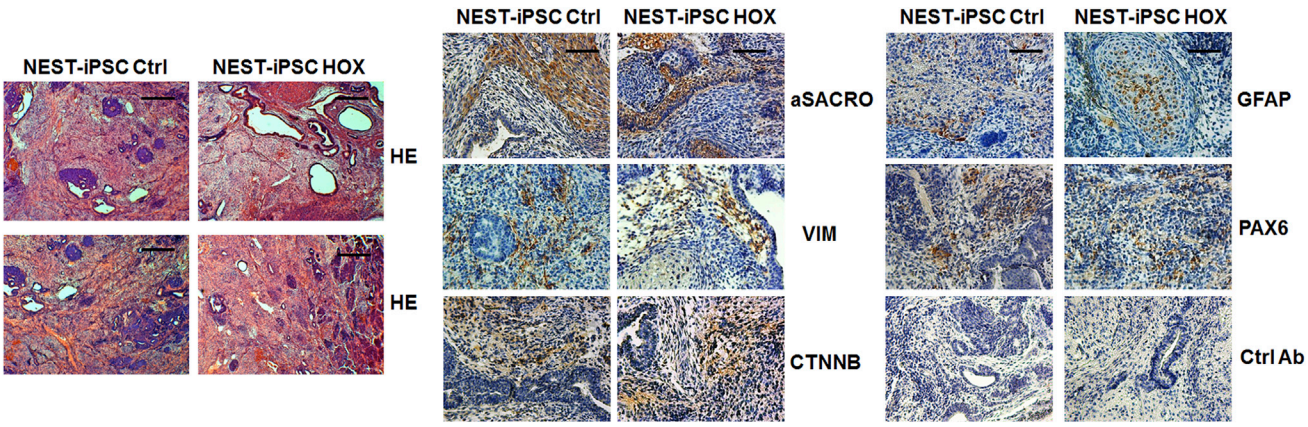

Figure 3. Pluripotency Analysis In Vivo: Teratoma Formation of Implanted NEST-iPSCs

Immature teratomas derived from control and *HOX*-transduced NEST-iPSCs were explanted 4–6 weeks after subcutaneous cell injection and further subjected to immunohistochemistry. H&E staining was performed to visualize the different cellular structures. The presence of derivatives of all three germ layers was further confirmed using specific antibodies to α-sarcomeric actin (aSACRO) and vimentin (VIM) (mesoderm), β-catenin (CTNNB) (endoderm), glial fibrillary acidic protein (GFAP), and PAX6 (ectoderm) in combination with 3,3′-diaminobenzidine (DAB) staining. Isotype controls (Ctrl Ab) were used as staining controls. Representative photographs for n = 3 different experiments are shown (n = 8–10 mice per group). Magnification, 40× (H&E) and 100× (DAB). Scale bars, 200 μm (H&E) and 100 μm (DAB).

flow-cytometric analysis (Figure 4B). Of note, the amounts of the NEST-reporter protein GFP and NEST itself were concomitantly increased, suggesting that ectopic *HOX* expression either mediated an increase of NEST/GFP expression or promoted the formation of NEST-GFP$^+$ cells during EB differentiation in vitro (Figure 4A). We also analyzed single-cell suspensions of control and *HOX*-transduced NEST-iPSCs by flow cytometry 2 days after transduction and of EBs after an additional 6 days (8 days after transduction) after intracellular staining for HOX, as well as expression of CD73 (Figure 4B). In agreement with the western blot analysis, HOXB7, HOXC6, and HOXC8 expressions were increased in NEST-iPSCs and EBs. The MSC-associated marker CD73 was somewhat increased relative to control in day-6 EBs.

Steady-state *HOX* transcription was further quantified by qRT-PCR (Figure 4C). As expected, significantly increased ectopic *HOXB7*, *HOXC6*, and *HOXC8* mRNA expressions were detected in transduced NEST-iPSCs using human-specific deoxyoligonucleotide primers for qRT-PCR. Interestingly, the overall relative amounts of transcripts were lower in day-6 EBs, probably due to retroviral vector silencing during iPSC differentiation, as reporter expression was also significantly reduced in EBs (Figure 4C; see also Figure 2E). Clustering global gene expression analysis showed that the gene expression profiles of ectopic *HOX*-expressing NEST-iPSCs and respective EBs were closer to those of VW-MSCs isolated from mouse aorta than those of control-transduced and EB-differentiated cells (Figure 4D).

Immunofluorescence as well as flow-cytometric analysis showed that ectopic *HOX* expression resulted in an increased number of NEST$^+$/GFP$^+$ cells during EB differentiation in vitro (Figures 5A and 5B). Immunofluorescence analysis was performed to visualize HOX protein as well as GFP marker protein expression (Figures 5C and S2). As expected, increased cytoplasmic as well as partially nuclear localization of the HOX proteins was observed in transduced and differentiated EB cells, as well as an increased immunoreactivity to the used lineage tracer GFP. Furthermore, to test for the propensity of the iPSC-derived MSCs to differentiate toward adipocytes and osteoblasts, we plated and cultured day-8 EBs in appropriate differentiation media for an additional 14 days (Figure 5D). Adipogenic as well as osteogenic differentiation of NEST-iPSCs-derived MSCs appeared to be more efficient when the three *HOX* genes were ectopically expressed. In vitro differentiation of *HOX*-transduced NEST-iPSCs toward multipotent MSCs and subsequent differentiation capabilities along the mesodermal lineage was further confirmed in TURQUOISE2$^+$-sorted NEST-iPSCs cultured on plastic for 7–10 days after transduction in the absence of leukemia inhibitory factor (LIF) (Figure 5E).

In summary, the ectopic expression of the three MSC-specific *HOX* genes promoted the in vitro differentiation of NEST-iPSCs toward GFP$^+$ multipotent MSCs.

Ectopic *HOX* Expression Promotes Formation of NEST-GFP$^+$, Vessel-Associated Mesenchymal Cells In Vivo

Interestingly, when originally evaluating pluripotency of the NEST-iPSCs, we observed increased masses and volumes of the teratomas when *HOXB7*, *HOXC6*, and *HOXC8* were ectopically expressed (Figure 6). Therefore,

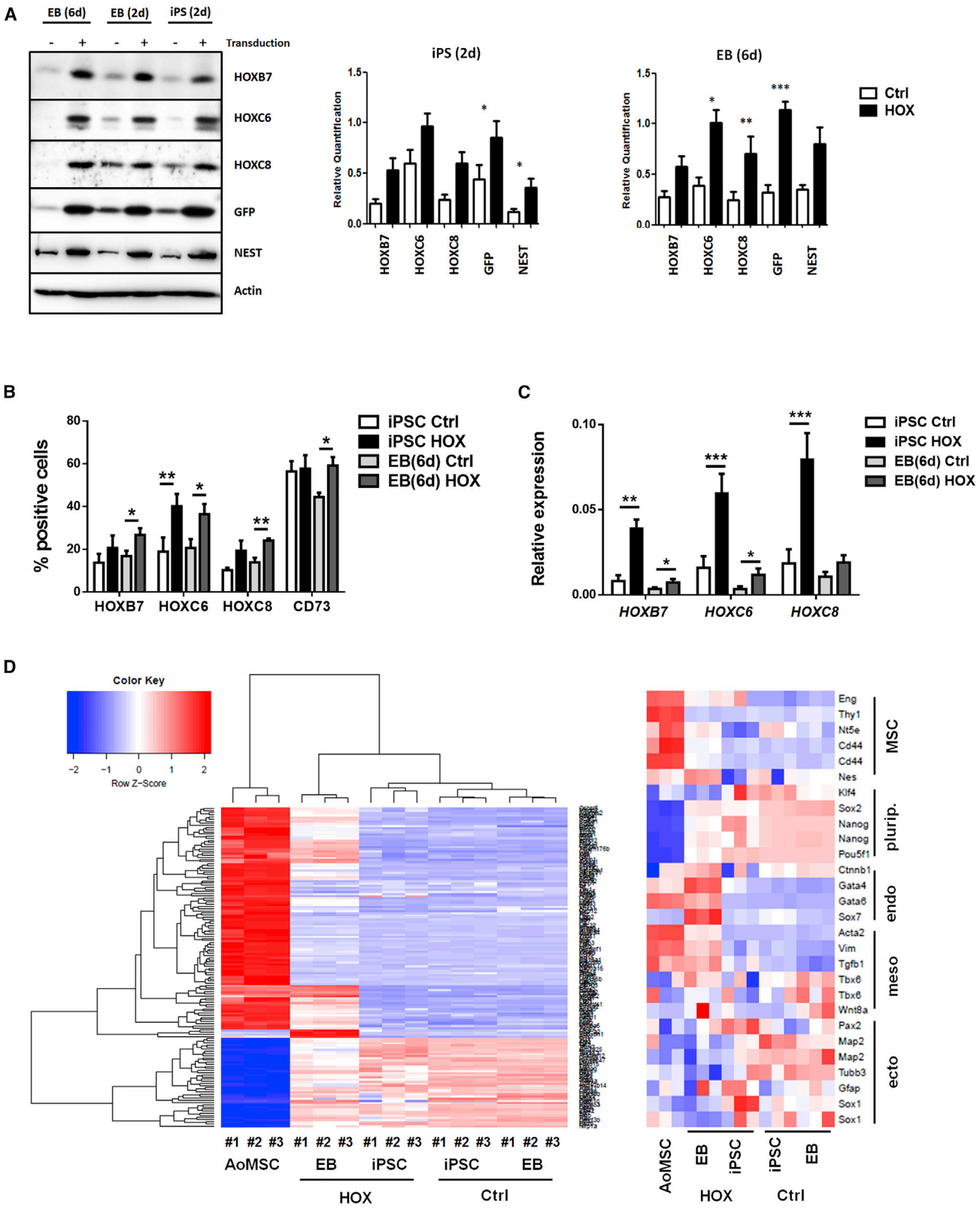

(legend on next page)

subcutaneous NEST-iPSC implantation was repeated and teratomas were removed 28 days post implantation. Indeed, tumor volumes and weights were significantly increased specifically in the *HOX* group (Figure 6A). Flow-cytometric analysis of cells of freshly isolated and dissociated tumors revealed a significantly increased proportion expressing the introduced *HOX* genes as well as cells expressing $NEST^{GFP}$ and the MSC marker CD90 (Figures 6B and S3). Accordingly, the amounts of HOX, GFP, and NEST proteins were higher in whole-tumor lysates from NEST-iPSC teratomas compared with control-transduced NEST-iPSCs (Figure 6C). In contrast, the amounts of VE-cadherin and PECAM1/CD31, two proteins expressed on endothelial cells, were not increased in the *HOX*-transduced teratomas, additionally indicating the specificity of these HOX proteins for MSC formation (Figures 6B and 6C). Immunofluorescence analysis of the vessel structure within the teratomas revealed that the vessels within tumors derived from *HOX*-transduced NEST-iPSCs were associated and surrounded by GFP^+ cells, which co-express mural cell markers (ACTA2) and clearly indicate vessel stabilization compared with the more immature vessels of the controls (Figures 7 and S4).

Taken together, our results strongly suggest the ectopic expression of MSC-specific *HOX* genes promotes differentiation of iPSCs toward $NEST^+$, multipotent MSCs which, in teratomas in vivo, preferentially associate with vessel structures.

DISCUSSION

HOX proteins are key regulators of the animal body plan controlling the expression of realizator genes, which themselves in turn impose positional identity to developing tissues (Mallo et al., 2010). The combined expression of a certain combination of *HOX* genes that specify a certain tissue has been termed the *HOX* code (Kessel and Gruss, 1991). We present here the directed generation of multipotent MSCs from reprogrammed pluripotent stem cells, in vitro, by ectopic expression of *HOXB7*, *HOXC6*, and *HOXC8*, based on a *HOX* code we have previously defined for VW-MSCs (Klein et al., 2013). We first generated iPSCs from skin fibroblasts of transgenic mice carrying a GFP gene under the control of the endogenous *Nest* promoter. Lentiviral expression of the aforementioned *HOX* coding sequences then efficiently promoted the formation of NEST-GFP^+ MSCs in differentiating EBs. Those cells displayed classical multipotent characteristics, in vitro, and selectively associated with vascular structures in NEST-iPSC teratomas in vivo, thus likely representing true VW-MSCs.

HOX genes are not only active during embryogenesis but are also involved in regeneration and repair of tissues throughout life (Wang et al., 2009). For example, cells with colony-forming unit (CFU) potential in the CFU-fibroblast assay, a retrospective readout frequently used to quantify MSC frequencies (Bianco et al., 2008), expresses different characteristic HOX gene signatures, depending on the organ/anatomical region from which they were isolated (Ackema and Charite, 2008; Sagi et al., 2012). During development and in particular during differentiation, the topographic specificity of *HOX* codes is maintained, which indicates that *HOX* expression patterns are an intrinsic property of MSCs and could probably also be used as a molecular fingerprint. In fact, we and others have demonstrated that stem and progenitor cells from mesodermal tissues display *HOX*-specific gene expression profiles. These fingerprints can be used to distinguish functionally distinct populations of MSCs, as has been demonstrated for bone marrow and umbilical cord blood (Liedtke et al., 2010). In particular, the *HOX* genes *HOXB7*, *HOXC6*, and *HOXC8* were strongly overexpressed in VW-resident MSCs in comparison with terminally differentiated endothelial cells,

Figure 4. *HOX*-Transduced NEST-iPSCs and Differentiated EBs Differentially Express HOXB7, HOXC6, and HOXC8 as well as the MSC Markers GFP and NESTIN

(A) Western blot analysis of indicated protein expressions were performed from whole-cell lysates of *HOX*-transduced and control NEST-iPSCs 2 days after transduction, and of aggregated EBs an additional 2 and 4 days after transduction. Representative blots (left panel) from at least n = 3 independent experiments are shown. Mean values ± SEM are shown for quantification (right panels) (biological replicates: NEST-iPSCs n = 7–11 per group [for nestin n = 4], EBs n = 7–11 per group [for nestin n = 3]); p values calculated by two-way ANOVA followed by post hoc Bonferroni test. *$p \leq 0.05$, **$p \leq 0.01$, ***$p \leq 0.005$.

(B) Single-cell suspensions of control and *HOX*-transduced NEST-iPSCs were analyzed 2 days after transduction and of EBs and after an additional 4 days by flow cytometry with the indicated antibodies. Data are presented as mean ± SEM (biological replicates: n = 6–8 for each epitope and group). *$p \leq 0.05$, **$p \leq 0.01$.

(C) Relative transcripts were further evaluated by qRT-PCR in iPSCs and in EBs (biological replicates: n = 6–9 per group and gene); p values calculated by two-way ANOVA followed by post hoc Bonferroni test. *$p \leq 0.05$, **$p \leq 0.01$, ***$p \leq 0.005$.

(D) Global gene expression heatmaps (left) of aorta-derived VW-MSCs and *HOX* as well as control-transduced NEST-iPSCs and differentiated EBs as determined by microarray analysis and selected MSC marker genes (right) with higher expressions in *HOX*-transduced and differentiated NEST-iPSC EBs and, thus, closer to aorta-derived VW-MSCs (biological replicates: n = 3 per group).

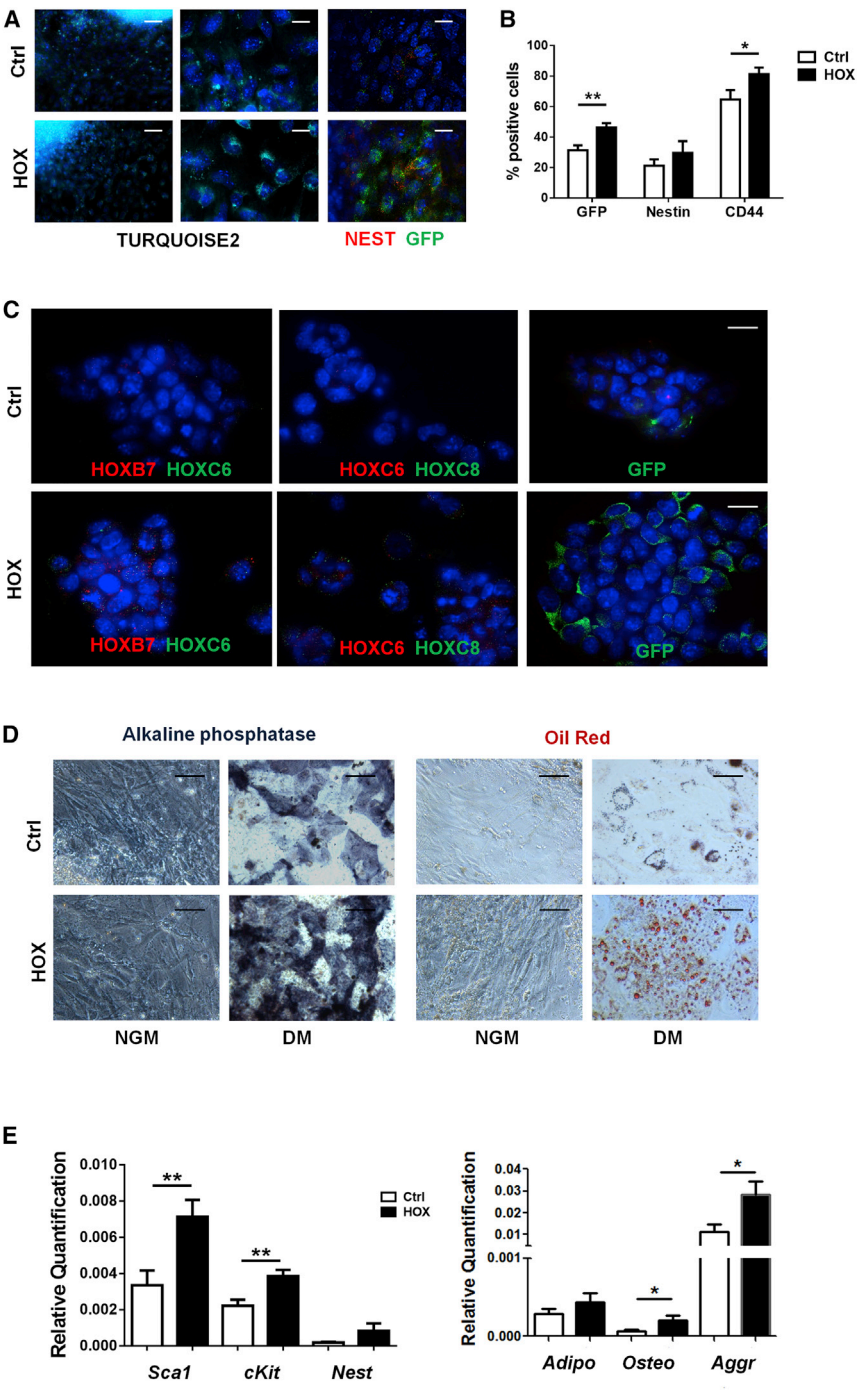

Figure 5. *HOX*-Transduced NEST-iPSCs and Differentiated EBs Differentiate into Cells of Mesodermal Lineages

(A) Reporter gene expression (TURQUOISE2 cyan fluorescence) was analyzed in *HOX*-transduced NEST-iPSCs and control-transduced (empty vector) NEST-iPSCs 96 hr after transduction by confocal microscopy. Cells were further stained for nestin (red) and GFP (green) marker expressions. Representative photographs of n = 4 independent experiments are shown. Scale bars, 100 μm (left panel) and 20 μm (middle and right panels).

(B) Single-cell suspensions of aggregated EBs generated from control and *HOX*-transduced NEST-iPSCs were analyzed by FACS for GFP, nestin, and MSC marker CD44 expressions. Data are presented as mean ± SEM (biological replicates: n = 6–8 for each epitope and group). *$p \leq 0.05$, **$p \leq 0.01$.

(C) Six days after transduction, aggregated EBs were seeded on gelatine-coated coverslips and immunofluorescence analysis for HOXB7, HOXC6, and HOXC8 expression was performed followed by confocal microscopy. Representative photographs from n = 4 independent experiments are shown. Scale bars, 15 μm.

(D) Verification of mesodermal differentiation. Dissociated 6-day EBs were subjected to in vitro differentiation into osteocytes and adipocytes. Differentiation was observed within 14 days after induction of differentiation as shown by oil red O staining and by histochemical staining for alkaline phosphatase. Representative photographs are shown (biological replicates: n = 6). Magnification, 400×. Scale bars, 25 μm.

(E) Selected MSC marker genes were further evaluated by qRT-PCR in TURQUOISE2^{+}-sorted iPSCs cultured on plastic for 7–10 days after transduction in the absence of LIF (biological replicates: n = 8 per group and gene). Trilineage differentiation along the mesodermal lineage was quantified after an additional 14 days of culture within differentiation medium by qRT-PCR analysis of adiponectin, osteocalcin, and aggrecan expression levels. Data are presented as mean ± SEM (biological replicates: n = 7 for each group and gene). *$p \leq 0.05$, **$p \leq 0.01$.

See also Figure S2.

SMCs, and pluripotent embryonic stem cells (Klein et al., 2013). This indicates that these genes are involved in the development and differentiation of the VW-resident MSCs. These MSCs typically reside in the adventitial vasculogenic zone, a specific stem cell niche of the vessel wall. A central hypothesis concerning these vessel-resident stem cells is that they are "first-line cells," which are a first point of contact for tumor cells and secreted factors because of

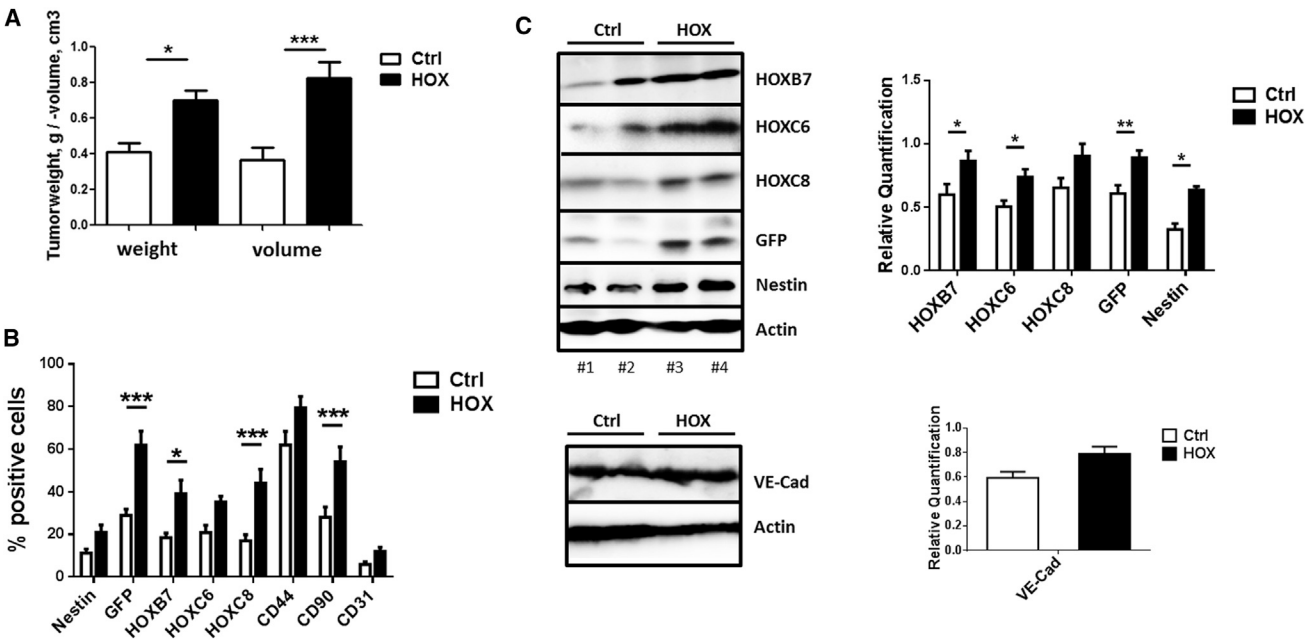

Figure 6. Comparative Analysis of Tumor Size and Quantitative Assessment of HOX Protein Expression in NEST-iPSC-Derived Teratomas

Control- and *HOX*-transduced NEST-iPSCs were subcutaneously transplanted into the flank of NMRI nude mice.

(A) Tumor weight and volume of explanted tumors were assessed 4 weeks after cell implantation. Data are presented as mean ± SEM from n = 3 independent experiments using at least five mice each (biological replicates: Ctrl n = 20, HOX n = 23; 43 mice in total); p values calculated by one-way ANOVA followed by post-hoc Tukey's test. *$p \leq 0.05$, ***$p \leq 0.005$.

(B) Ex vivo isolated tumors were digested with collagenase and single-cell suspensions were analyzed by FACS with indicated antibodies. Data are presented as mean ± SEM (biological replicates: n = 8–10 for each epitope and group); p values calculated by two-way ANOVA followed by post hoc Bonferroni test. *$p \leq 0.05$, ***$p \leq 0.005$.

(C) Expression levels of the indicated proteins were analyzed and quantified in whole-tumor protein lysates using western blot analysis (biological replicates: n = 15–20 for each protein and group [VE-cadherin n = 6]); p values calculated by two-way ANOVA followed by post hoc Bonferroni test. *$p \leq 0.05$, **$p \leq 0.01$.

See also Figure S3.

their anatomical location (Ergun et al., 2011). In this regard it was recently shown that tissue-resident MSCs that predominantly reside in the adventitial vasculogenic zone of adult blood vessels—and not those from the bone marrow—can be mobilized from their niche, for example by signals released from tumor cells. These cells then contribute to vascular remodeling of tumor blood vessels by differentiating into pericytes as well as SMCs, which in turn stabilize angiogenic blood vessels (Ergun et al., 2011; Klein et al., 2011, 2014). Without mobilization from the niche, VW-resident MSCs express the *HOXB7*, *HOXC6*, and *HOXC8* genes at high level whereas expression of transgelin (tagln), an essential factor in early SMC differentiation, is repressed. Upon mobilization and pericyte/SMC differentiation, these three VW-MSC-specific *HOX* genes were silenced (Klein et al., 2013). Silencing of these genes resulted in alterations of CpG methylation of the *Tagln* promoter, leading to increased TAGLN expression, which was associated with induction of VW-MSC differentiation into SMC/pericytes (Klein et al., 2013). In this work, we used the three VW-MSC-specific genes *HOXB7*, *HOXC6*, and *HOXC8* to test whether their enforced expression would program differentiating iPSCs toward vessel wall-typical multipotent MSCs. Indeed, this triple combination resulted in a significantly increased number of NEST-GFP$^+$ MSCs. In vitro, the obtained cells adhered to plastic and could be differentiated along different mesodermal lineages, thus providing strong evidence for their multipotency and MSC-like differentiation potential. Moreover, the generated cells also showed classical MSC-like behavior in teratomas in vivo. They were found to be associated with newly formed blood vessels, which nicely correlated with the observed increased size of the teratomas grown from *HOX*-transduced NEST-iPSCs. Tissue-resident NEST$^+$ MSCs have already been shown to be essential for vessel stabilization during neovascularization processes and serve as a local source for pericytes and SMCs (Klein et al., 2014).

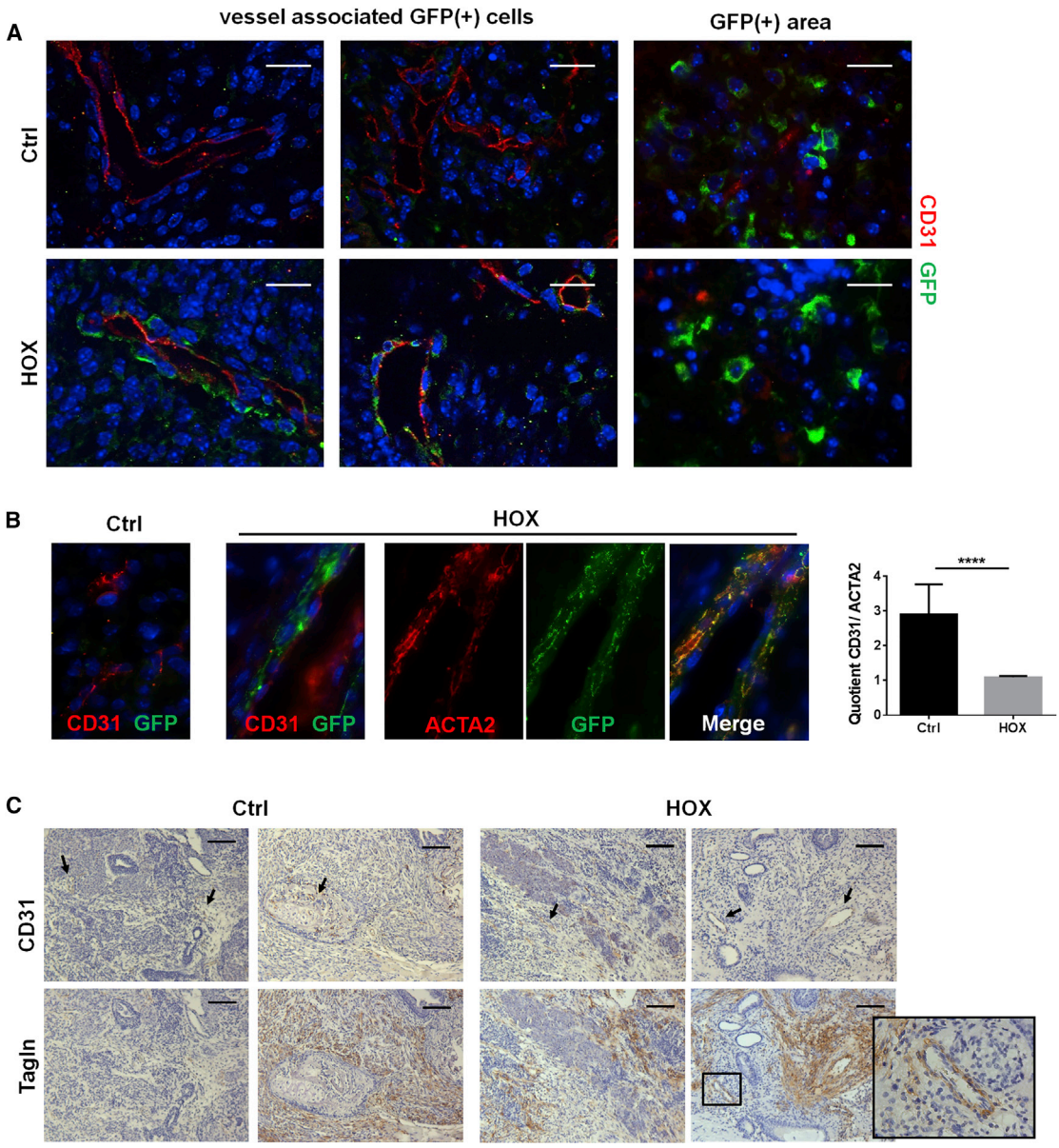

Figure 7. Differentiated NEST-GFP$^+$ Cells Associate with Angiogenic Vessels in *HOX*-Transduced NEST-iPSC-Derived Teratomas

Subcutaneously grown tumors were analyzed by immunofluorescence and confocal microscopy.

(A) Sections were stained for CD31/PECAM (red) and GFP (green). Representative images of n = 4 independent experiments are shown. Magnification, 63×. Scale bars, 20 μm.

(B) Higher-magnification images (magnification 63×). CD31- and ACTA2-positive vessels were quantified by counting respective immune-reactive vascular structures in whole-tumor sections. Vessels were quantified by counting in at least three whole cross-sections per tumor, and averages for individual animals were calculated. Depicted data represent the mean values of all mice per group (n = 6 mice per group). ****$p \leq 0.001$.

(C) Teratoma sections were further stained for CD31 (indicated by arrows) and ACTA2 using DAB staining (brown). Scale bars, 200 μm. See also Figure S4.

Given the importance of the master regulatory *HOX* genes for patterning during embryogenesis, we expect that the ectopic expression of a specific *HOX* code could allow for enhanced development of desired tissues in vitro. One example is human *HOXB4*, which is highly expressed in the hematopoietic stem and progenitor cell compartment in the adult bone marrow. Its ectopic expression in differentiating mouse embryonic stem cells

promotes the formation of long-term repopulating hematopoietic stem cells in vitro (Pilat et al., 2005, 2013).

Several studies have already successfully reported the generation of MSCs from human iPSCs using special media formulations (Chen et al., 2012; Frobel et al., 2014; Sheyn et al., 2016). However, in this work we present the successful direct programming of iPSCs toward VW-typical MSCs by ectopic expression of a small set of *HOX* genes, namely *HOXB7*, *HOXC6*, and *HOXC8*. As the activity of homeotic selector proteins are highly conserved throughout evolution, it is very likely that our results will also hold true for human iPSCs. The possibility and feasibility of obtaining patient-specific VW-MSCs from iPSCs in large amounts by forward programming could potentially open avenues toward novel, MSC-based therapies. Finally, it remains to be shown whether this approach could also be used for enforcing transdifferentiation of other somatic cell types toward MSCs, thus avoiding the need for prior reprogramming of those cells back to the pluripotent stage.

EXPERIMENTAL PROCEDURES

Reprogramming of Mouse NEST-GFP Tail-Tip Fibroblasts

Fibroblast cultures (see Supplemental Experimental Procedures) were established and reprogrammed using a lentiviral vector co-expressing the coding sequences of *POU5F1*, *KLF4*, *MYC*, and *SOX2* together with the gene encoding tomato fluorescent protein. Vector particle production (see Supplemental Experimental Procedures) was performed as previously described (Stanurova et al., 2016). Primary fibroblasts were cultured up to 80% confluence. Fibroblasts were trypsinized, counted, and adjusted to a density of 1×10^5 in 150 μL of Dulbecco's modified Eagle's medium (DMEM, high glucose) with 10% fetal bovine serum, 1% sodium pyruvate and 50 units/mL penicillin/streptomycin (nTTF medium). Protamine sulfate (4 μg/mL) and virus according to an MOI of 10 was added to the cell suspension, which was then seeded at a density of 4,000 cells/cm^2. Medium was completely exchanged 24 hr later. Two days after transduction, cells expressing tomato fluorescent protein were isolated by fluorescence-activated cell sorting and plated at a density of 1,500 cells/cm^2 on γ-irradiated mouse embryonic fibroblasts in 6-well plate in mouse iPSC medium (KO-DMEM, 15% [v/v] pretested fetal calf serum [FCS], leukemia inhibitory factor [mouse recombinant LIF, final concentration 10 ng/mL or conditioned medium], penicillin/streptomycin, L-Gln, and monothioglycerol [MTG; final concentration 1.5×10^{-4} M]). All media, PBS, and supplements were obtained from Life Technologies unless otherwise stated. Cells were kept at 37°C, atmospheric O_2 partial pressure, and 5% CO_2 in a humidified incubator. Colonies were picked approximately 2 weeks post transduction, and generated NEST-GFP iPSCs (NEST-iPSCs) were sorted by flow cytometry (dtTomato$^-$ and SSEA1$^+$) as single cells and clonally expanded. Single clones were further expanded feeder-layer free on gelatine-coated dishes in mouse iPSC medium containing LIF.

HOX Gene Expression Vector and Transduction

Generated NEST-GFP iPSCs were transduced using a lentiviral SIN vector co-expressing the coding sequences of *HOXB7*, *HOXC6*, and *HOXC8* separated by *2A esterase* elements together with the gene encoding Turquoise2 (cyan) fluorescent protein (see Supplemental Experimental Procedures). For this purpose, vector-containing supernatants were collected from HEK293 cells transfected with 5 μg of pRRL.PPT.SF.HOXB7.2A.C6L.2A.C8.2A.Turq plasmid or 5 μg of control plasmid (same vector without the HOX genes) mixed with 15 μg of wild-type Gag-Pol plasmid (MLV_SynGag) and 2 μg of pMDG-VSVG plasmid (pMDG) encoding the envelope protein. Vectors were concentrated by ultracentrifugation. iPSCs were seeded as single cells at a density of 1×10^4 cells/cm^2 onto gelatine-coated 6-well plates and cultured in iPSC medium with 50 μL of vector-containing supernatant. For formation of hanging-drop EBs (48 hr after transduction), single-cell drops (2,000 cells/20 μL) were hanging-cultured on the lid of Petri dishes as described elsewhere (Lin et al., 2014). After another 48 hr (EBs formed with uniform size) aggregated EBs were washed off and plated in 6-well plastic plates, and MSC differentiation was further induced by culturing in MSC medium (complete DMEM supplemented with 20% FCS) or PAN-MSC medium (P08-50200, PAN Biotech).

Teratoma Formation Assay

This study was carried out in strict accordance with the recommendations of the Guide for the Care and Use of Laboratory Animals of the German Government. All procedures involving mice were approved by the local institutional Animal Care Committee (Regierungspräsidium Düsseldorf Az84-02.04.2012.A285; Az84-02.04.2016.A010). Mice were kept under standard conditions in the Central Animal Facility of the University Hospital, Essen. iPSCs for injection were harvested by incubation with Accutase (Life Technologies) for 15 min at 37°C to generate a single-cell suspension. After washing with PBS, cells were resuspended in DMEM/F12 supplemented with 50% growth-factor-reduced Matrigel (BD Bioscience) at a density of 1×10^7 cells/mL. Xenograft teratomas were generated by subcutaneous injection of 1×10^6 cells/mL of iPSCs into both hindlimbs of immunodeficient NMRI nu/nu mice (Harlan Laboratories). Mice were monitored daily for teratoma growth. Tumors were explanted when apparent skin lesions appeared, tumors reached a critical size, or at latest 60 days after injection. Mice were killed by isoflurane euthanasia. Tumors were explanted and divided. One half was fixed in 4% paraformaldehyde overnight and embedded in paraffin. The other half was snap-frozen in liquid nitrogen and stored at −80°C or subjected to single-cell suspension (see Supplemental Experimental Procedures). For teratoma histopathology, 5-μm paraffin cross-sections were taken at the midpoint through the block. Sections were stained with H&E for histological evaluation.

Immunohistochemistry and Immunofluorescence

Paraffin-embedded tissue sections were hydrated using a descending alcohol series, incubated for 10–20 min in target retrieval solution (Dako), and incubated with blocking solution (2% FCS/PBS). After permeabilization, sections were incubated with primary antibodies overnight at 4°C. Antigens were detected with anti-rabbit Alexa 488- and anti-mouse Alexa 555-conjugated secondary antibodies (1:500). DAPI was used to stain nuclei. Cells were cultured

on gelatine-coated coverslips and fixed prior to staining using 4% paraformaldehyde for 15 min at room temperature. For staining of nuclear proteins, cells were permeabilized by incubation in 0.1% (v/v) Triton X-100 for 5 min at room temperature. After washing and blocking in PBS with 2% normal goat serum (serum of secondary antibody host species; Cell Signaling Technology), incubation with the primary antibody was carried out for 2–4 hr at room temperature. After washing with PBS, fluorescently labeled secondary antibodies were applied for 2 hr. Specimens were embedded in fluorescent mounting medium (Dako) and imaged on a Zeiss Axioserver fluorescence microscope using the Axiovision acquisition software from Zeiss.

Microarray-Based Gene Expression Analysis and Hierarchical Clustering

VW-resident MSCs were isolated from aortas of C57BL/6-Tg(CAG-EGFP)1Osb/J mice (Jackson Laboratory) as previously described (Klein et al., 2014, 2016a, 2016b) Total RNA was isolated from these cells as well as from control and *HOX*-transduced NEST-iPSCs 2 days after transduction and from generated EBs after an additional 6 days (8 days after transduction) (n = 3 for each group). Total RNA integrity was assessed using a 2100 Bioanalyzer (Agilent Technologies) in combination with the RNA 6000 Nano Kit (Agilent Technologies): all samples showed an RNA integrity number of >8.5. Global gene expression profiling was performed using SurePrint G3 Mouse Gene Expression 8 × 60 k microarrays (AMADID 028005, Agilent Technologies) according to the manufacturer's protocol with an input of 50 ng of total RNA (one-color Low Input Quick Amp Labeling Kit, Agilent Technologies). Hybridized microarrays were scanned with a G2505C Sure Scan Microarray Scanner (Agilent Technologies) and raw data were extracted with Feature Extraction 10.7 software (Agilent Technologies). Data quality assessment, preprocessing, normalization, and differential expression analyses were conducted using the R Bioconductor packages limma (Ritchie et al., 2015) and Agi4x44PreProcess, whereas Benjamini-Hochberg adjusted p values (false discovery rate) smaller than 0.5 were considered statistically significant (Benjamini and Hochberg, 1995). Unsupervised hierarchical clustering and visualization was performed on gene expression *Z* scores using the heatmap.2 function from the R package gplots (https://cran.r-project.org/web/packages/gplots/index.html) with standard options (Euclidian clustering distance and clustering function "complete").

Statistical Analysis

Unless otherwise indicated, data were obtained from three independent experiments (n = 3). Mean values were calculated and used for analysis of SD or SEM as indicated. Statistical significance was evaluated by one- or two-way ANOVA followed by Tukey's or Bonferroni's multiple comparisons post test as indicated. Statistical significance was set at the level of $p \leq 0.05$ (*$p \leq 0.05$, **$p \leq 0.01$, $^{\#,}$ ***$p \leq 0.005$, ****$p \leq 0.001$ in the figures). Data analysis was performed with Prism 5.0 software (GraphPad).

ACCESSION NUMBERS

The accession number for the microarray data reported in this article is ArrayExpress: E-MTAB-5565.

SUPPLEMENTAL INFORMATION

Supplemental Information includes Supplemental Experimental Procedures, four figures, and three tables and can be found with this article online at http://dx.doi.org/10.1016/j.stemcr.2017.03.001.

AUTHOR CONTRIBUTIONS

J.S., M.Z., M.B., L.B., N.T., A.G., H.K., and D.K. performed experiments; J.H. and K.U. performed microarray analyses; H.K. and D.K. supervised and analyzed results and made the figures; H.K. and D.K. designed research and wrote the paper. All authors read and approved the manuscript.

ACKNOWLEDGMENTS

We thank V. Jendrossek and P. Horn for hosting our groups and their support in this project. We also thank I. Spratte and S. Skibbe for excellent technical assistance and K. Lennartz for the help with FACS. The work was supported by the UK Essen/IFORES (D/107-81040, D.K.) and BMBF FKZ 01GN0815 (M.Z.).

Received: December 4, 2016
Revised: March 5, 2017
Accepted: March 6, 2017
Published: March 30, 2017

REFERENCES

Ackema, K.B., and Charite, J. (2008). Mesenchymal stem cells from different organs are characterized by distinct topographic Hox codes. Stem Cells Dev. *17*, 979–991.

Benjamini, Y., and Hochberg, Y. (1995). Controlling the false discovery rate: a practical and powerful approach to multiple testing. J. R. Stat. Soc. Series B Stat. Methodol. *57*, 289–300.

Bianco, P., Robey, P.G., and Simmons, P.J. (2008). Mesenchymal stem cells: revisiting history, concepts, and assays. Cell Stem Cell *2*, 313–319.

Chen, Y.S., Pelekanos, R.A., Ellis, R.L., Horne, R., Wolvetang, E.J., and Fisk, N.M. (2012). Small molecule mesengenic induction of human induced pluripotent stem cells to generate mesenchymal stem/stromal cells. Stem Cells Transl. Med. *1*, 83–95.

Ergun, S., Tilki, D., and Klein, D. (2011). Vascular wall as a reservoir for different types of stem and progenitor cells. Antioxid. Redox Signal. *15*, 981–995.

Frobel, J., Hemeda, H., Lenz, M., Abagnale, G., Joussen, S., Denecke, B., Saric, T., Zenke, M., and Wagner, W. (2014). Epigenetic rejuvenation of mesenchymal stromal cells derived from induced pluripotent stem cells. Stem Cell Rep. *3*, 414–422.

Galipeau, J. (2013). The mesenchymal stromal cells dilemma—does a negative phase III trial of random donor mesenchymal stromal cells in steroid-resistant graft-versus-host disease represent a death knell or a bump in the road? Cytotherapy *15*, 2–8.

Gibbons, G.H., and Dzau, V.J. (1994). The emerging concept of vascular remodeling. N. Engl. J. Med. *330*, 1431–1438.

Gotherstrom, C., West, A., Liden, J., Uzunel, M., Lahesmaa, R., and Le Blanc, K. (2005). Difference in gene expression between human

fetal liver and adult bone marrow mesenchymal stem cells. Haematologica *90*, 1017–1026.

Ho, P.J., Yen, M.L., Tang, B.C., Chen, C.T., and Yen, B.L. (2013). H2O2 accumulation mediates differentiation capacity alteration, but not proliferative decline, in senescent human fetal mesenchymal stem cells. Antioxid. Redox Signal. *18*, 1895–1905.

Janzen, V., Forkert, R., Fleming, H.E., Saito, Y., Waring, M.T., Dombkowski, D.M., Cheng, T., DePinho, R.A., Sharpless, N.E., and Scadden, D.T. (2006). Stem-cell ageing modified by the cyclin-dependent kinase inhibitor p16INK4a. Nature *443*, 421–426.

Jin, H.J., Bae, Y.K., Kim, M., Kwon, S.J., Jeon, H.B., Choi, S.J., Kim, S.W., Yang, Y.S., Oh, W., and Chang, J.W. (2013). Comparative analysis of human mesenchymal stem cells from bone marrow, adipose tissue, and umbilical cord blood as sources of cell therapy. Int. J. Mol. Sci. *14*, 17986–18001.

Jung, Y., Bauer, G., and Nolta, J.A. (2012). Concise review: induced pluripotent stem cell-derived mesenchymal stem cells: progress toward safe clinical products. Stem Cells *30*, 42–47.

Kessel, M., and Gruss, P. (1991). Homeotic transformations of murine vertebrae and concomitant alteration of Hox codes induced by retinoic acid. Cell *67*, 89–104.

Kimbrel, E.A., Kouris, N.A., Yavanian, G.J., Chu, J., Qin, Y., Chan, A., Singh, R.P., McCurdy, D., Gordon, L., Levinson, R.D., et al. (2014). Mesenchymal stem cell population derived from human pluripotent stem cells displays potent immunomodulatory and therapeutic properties. Stem Cells Dev. *23*, 1611–1624.

Klein, D. (2016). Vascular wall-resident multipotent stem cells of mesenchymal nature within the process of vascular remodeling: cellular basis, clinical relevance, and implications for stem cell therapy. Stem Cell Int. *2016*, 1905846.

Klein, D., Weisshardt, P., Kleff, V., Jastrow, H., Jakob, H.G., and Ergun, S. (2011). Vascular wall-resident CD44+ multipotent stem cells give rise to pericytes and smooth muscle cells and contribute to new vessel maturation. PLoS One *6*, e20540.

Klein, D., Benchellal, M., Kleff, V., Jakob, H.G., and Ergun, S. (2013). Hox genes are involved in vascular wall-resident multipotent stem cell differentiation into smooth muscle cells. Sci. Rep. *3*, 2178.

Klein, D., Meissner, N., Kleff, V., Jastrow, H., Yamaguchi, M., Ergun, S., and Jendrossek, V. (2014). NESTin(+) tissue-resident multipotent stem cells contribute to tumor progression by differentiating into pericytes and smooth muscle cells resulting in blood vessel remodeling. Front. Oncol. *4*, 169.

Klein, D., Schmetter, A., Imsak, R., Wirsdorfer, F., Unger, K., Jastrow, H., Stuschke, M., and Jendrossek, V. (2016a). Therapy with multipotent mesenchymal stromal cells protects lungs from radiation-induced injury and reduces the risk of lung metastasis. Antioxid. Redox Signal. *24*, 53–69.

Klein, D., Steens, J., Wiesemann, A., Schulz, F.C., Kaschani, F., Roeck, K., Yamaguchi, M., Wirsdorfer, F., Kaiser, M., Fischer, J., et al. (2016b). Mesenchymal stem cell therapy protects lungs from radiation-induced endothelial cell loss by restoring superoxide dismutase 1 expression. Antioxid. Redox Signal. http://dx.doi.org/10.1089/ars.2016.6748.

Korshunov, V.A., Schwartz, S.M., and Berk, B.C. (2007). Vascular remodeling: hemodynamic and biochemical mechanisms underlying Glagov's phenomenon. Arterioscler. Thromb. Vasc. Biol. *27*, 1722–1728.

Kyriakou, C., Rabin, N., Pizzey, A., Nathwani, A., and Yong, K. (2008). Factors that influence short-term homing of human bone marrow-derived mesenchymal stem cells in a xenogeneic animal model. Haematologica *93*, 1457–1465.

Liedtke, S., Buchheiser, A., Bosch, J., Bosse, F., Kruse, F., Zhao, X., Santourlidis, S., and Kogler, G. (2010). The HOX Code as a "biological fingerprint" to distinguish functionally distinct stem cell populations derived from cord blood. Stem Cell Res. *5*, 40–50.

Lin, Y., Li, X.Y., Willis, A.L., Liu, C., Chen, G., and Weiss, S.J. (2014). Snail1-dependent control of embryonic stem cell pluripotency and lineage commitment. Nat. Commun. *5*, 3070.

Lindvall, O., and Kokaia, Z. (2010). Stem cells in human neurodegenerative disorders—time for clinical translation? J. Clin. Invest. *120*, 29–40.

Liu, Y., Goldberg, A.J., Dennis, J.E., Gronowicz, G.A., and Kuhn, L.T. (2012). One-step derivation of mesenchymal stem cell (MSC)-like cells from human pluripotent stem cells on a fibrillar collagen coating. PLoS One *7*, e33225.

Mallo, M., Wellik, D.M., and Deschamps, J. (2010). Hox genes and regional patterning of the vertebrate body plan. Dev. Biol. *344*, 7–15.

Mimeault, M., and Batra, S.K. (2009). Recent insights into the molecular mechanisms involved in aging and the malignant transformation of adult stem/progenitor cells and their therapeutic implications. Ageing Res. Rev. *8*, 94–112.

Miura, M., Miura, Y., Padilla-Nash, H.M., Molinolo, A.A., Fu, B., Patel, V., Seo, B.M., Sonoyama, W., Zheng, J.J., Baker, C.C., et al. (2006). Accumulated chromosomal instability in murine bone marrow mesenchymal stem cells leads to malignant transformation. Stem Cells *24*, 1095–1103.

Montesinos, J.J., Flores-Figueroa, E., Castillo-Medina, S., Flores-Guzman, P., Hernandez-Estevez, E., Fajardo-Orduna, G., Orozco, S., and Mayani, H. (2009). Human mesenchymal stromal cells from adult and neonatal sources: comparative analysis of their morphology, immunophenotype, differentiation patterns and neural protein expression. Cytotherapy *11*, 163–176.

Nauta, A.J., and Fibbe, W.E. (2007). Immunomodulatory properties of mesenchymal stromal cells. Blood *110*, 3499–3506.

Okano, H., Nakamura, M., Yoshida, K., Okada, Y., Tsuji, O., Nori, S., Ikeda, E., Yamanaka, S., and Miura, K. (2013). Steps toward safe cell therapy using induced pluripotent stem cells. Circ. Res. *112*, 523–533.

Pilat, S., Carotta, S., Schiedlmeier, B., Kamino, K., Mairhofer, A., Will, E., Modlich, U., Steinlein, P., Ostertag, W., Baum, C., et al. (2005). HOXB4 enforces equivalent fates of ES-cell-derived and adult hematopoietic cells. Proc. Natl. Acad. Sci. USA *102*, 12101–12106.

Pilat, S., Carotta, S., and Klump, H. (2013). Development of hematopoietic stem and progenitor cells from mouse embryonic stem cells, in vitro, supported by ectopic human HOXB4 expression. Methods Mol. Biol. *1029*, 129–147.

Pittenger, M.F., Mackay, A.M., Beck, S.C., Jaiswal, R.K., Douglas, R., Mosca, J.D., Moorman, M.A., Simonetti, D.W., Craig, S., and Marshak, D.R. (1999). Multilineage potential of adult human mesenchymal stem cells. Science *284*, 143–147.

Prasanna, S.J., Gopalakrishnan, D., Shankar, S.R., and Vasandan, A.B. (2010). Pro-inflammatory cytokines, IFNgamma and TNFalpha, influence immune properties of human bone marrow and Wharton jelly mesenchymal stem cells differentially. PLoS One *5*, e9016.

Renna, N.F., de Las Heras, N., and Miatello, R.M. (2013). Pathophysiology of vascular remodeling in hypertension. Int. J. Hypertens. *2013*, 808353.

Ribeiro, A., Laranjeira, P., Mendes, S., Velada, I., Leite, C., Andrade, P., Santos, F., Henriques, A., Graos, M., Cardoso, C.M., et al. (2013). Mesenchymal stem cells from umbilical cord matrix, adipose tissue and bone marrow exhibit different capability to suppress peripheral blood B, natural killer and T cells. Stem Cell Res. Ther. *4*, 125.

Ritchie, M.E., Phipson, B., Wu, D., Hu, Y., Law, C.W., Shi, W., and Smyth, G.K. (2015). Limma powers differential expression analyses for RNA-sequencing and microarray studies. Nucleic Acids Res. *43*, e47.

Rombouts, W.J., and Ploemacher, R.E. (2003). Primary murine MSC show highly efficient homing to the bone marrow but lose homing ability following culture. Leukemia *17*, 160–170.

Sagi, B., Maraghechi, P., Urban, V.S., Hegyi, B., Szigeti, A., Fajka-Boja, R., Kudlik, G., Nemet, K., Monostori, E., Gocza, E., et al. (2012). Positional identity of murine mesenchymal stem cells resident in different organs is determined in the postsegmentation mesoderm. Stem Cells Dev. *21*, 814–828.

Schu, S., Nosov, M., O'Flynn, L., Shaw, G., Treacy, O., Barry, F., Murphy, M., O'Brien, T., and Ritter, T. (2012). Immunogenicity of allogeneic mesenchymal stem cells. J. Cell Mol. Med. *16*, 2094–2103.

Sheyn, D., Ben-David, S., Shapiro, G., De Mel, S., Bez, M., Ornelas, L., Sahabian, A., Sareen, D., Da, X., Pelled, G., et al. (2016). Human iPSCs differentiate into functional MSCs and repair bone defects. Stem Cells Transl. Med. *5*, 1447–1460.

Stanurova, J., Neureiter, A., Hiber, M., de Oliveira Kessler, H., Stolp, K., Goetzke, R., Klein, D., Bankfalvi, A., Klump, H., and Steenpass, L. (2016). Angelman syndrome-derived neurons display late onset of paternal UBE3A silencing. Sci. Rep. *6*, 30792.

Tyndall, A. (2014). Mesenchymal stem cell treatments in rheumatology: a glass half full? Nat. Rev. Rheumatol. *10*, 117–124.

Wagner, W., and Ho, A.D. (2007). Mesenchymal stem cell preparations—comparing apples and oranges. Stem Cell Rev. *3*, 239–248.

Wang, K.C., Helms, J.A., and Chang, H.Y. (2009). Regeneration, repair and remembering identity: the three Rs of Hox gene expression. Trends Cell Biol. *19*, 268–275.

Wang, X., Kimbrel, E.A., Ijichi, K., Paul, D., Lazorchak, A.S., Chu, J., Kouris, N.A., Yavanian, G.J., Lu, S.J., Pachter, J.S., et al. (2014). Human ESC-derived MSCs outperform bone marrow MSCs in the treatment of an EAE model of multiple sclerosis. Stem Cell Rep. *3*, 115–130.

Wegmeyer, H., Broske, A.M., Leddin, M., Kuentzer, K., Nisslbeck, A.K., Hupfeld, J., Wiechmann, K., Kuhlen, J., von Schwerin, C., Stein, C., et al. (2013). Mesenchymal stromal cell characteristics vary depending on their origin. Stem Cells Dev. *22*, 2606–2618.

Zhang, Z.Y., Teoh, S.H., Chong, M.S., Schantz, J.T., Fisk, N.M., Choolani, M.A., and Chan, J. (2009). Superior osteogenic capacity for bone tissue engineering of fetal compared with perinatal and adult mesenchymal stem cells. Stem Cells *27*, 126–137.

Zhu, Y., Yang, Y., Zhang, Y., Hao, G., Liu, T., Wang, L., Yang, T., Wang, Q., Zhang, G., Wei, J., et al. (2014). Placental mesenchymal stem cells of fetal and maternal origins demonstrate different therapeutic potentials. Stem Cell Res. Ther. *5*, 48.

Stem Cell Reports, Volume *8*

Supplemental Information

In Vitro Generation of Vascular Wall-Resident Multipotent Stem Cells of Mesenchymal Nature from Murine Induced Pluripotent Stem Cells

Jennifer Steens, Melanie Zuk, Mohamed Benchellal, Lea Bornemann, Nadine Teichweyde, Julia Hess, Kristian Unger, André Görgens, Hannes Klump, and Diana Klein

1. Supplemental Figures

Figure S1

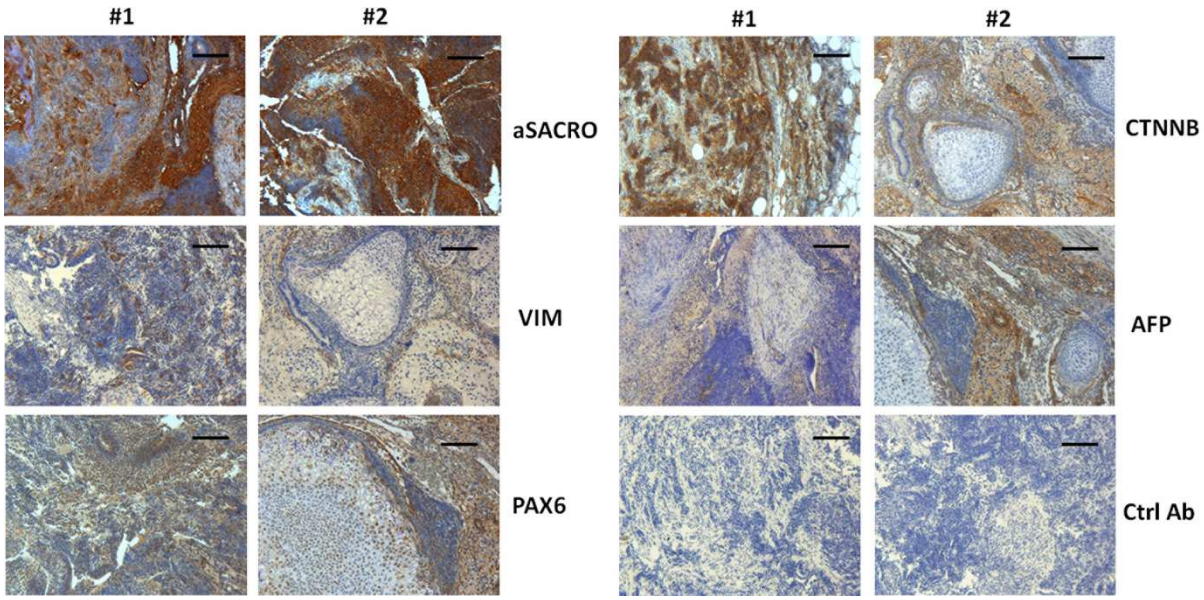

Supplemental Figure S1. Related to Figure 1.

Pluripotency analysis in vivo: teratoma formation of implanted NEST-iPSCs clones.

Immature teratomas derived from two different NEST-iPSCs clones (#1, #2) were explanted 4 weeks after subcutaneous cell injection and further subjected to immunohistochemistry. The presence of derivatives of all three germ layers was further confirmed using specific antibodies to alpha-sacromeric actin and vimentin (mesoderm), beta-catenin and alpha-fetoprotein (endoderm), and PAX6 (ectoderm) in combination with DAB staining. Mouse IgG1 isotype controls (Ctrl Ab) were used as staining controls. Representative photographs of n=6 independent experiments are shown Magnification 100x (scale bars 100 µm).

Figure S2

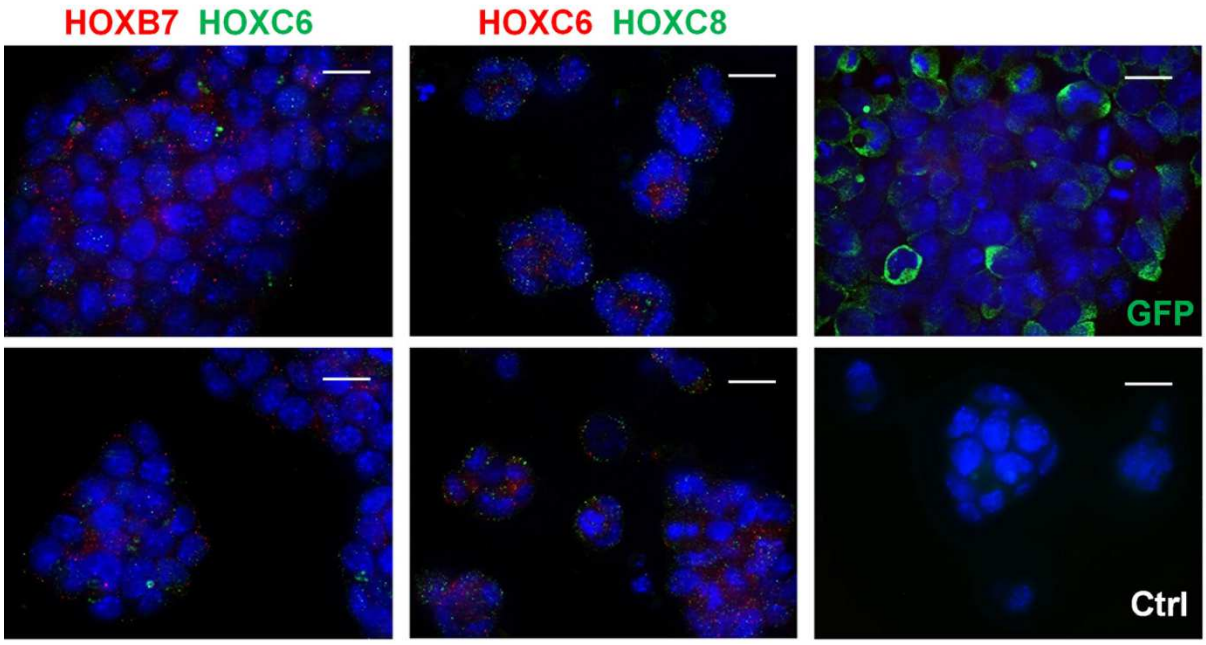

Supplemental Figure S2. Related to Figure 5.

Confocal microscopy of fluorescently labelled *HOX*-transduced NEST-iPSCs and subsequently differentiated EBs.

Six days after transduction, aggregated EBs were seeded on gelatine-coated cover-slips and immunofluorescence analysis for HOXB7, HOXC6 and HOXC8 as well as GFP expression was performed followed by confocal microscopy. Representative images of n=4 independent experiments are shown**.** Scale bar: 15 µm.

Figure S3

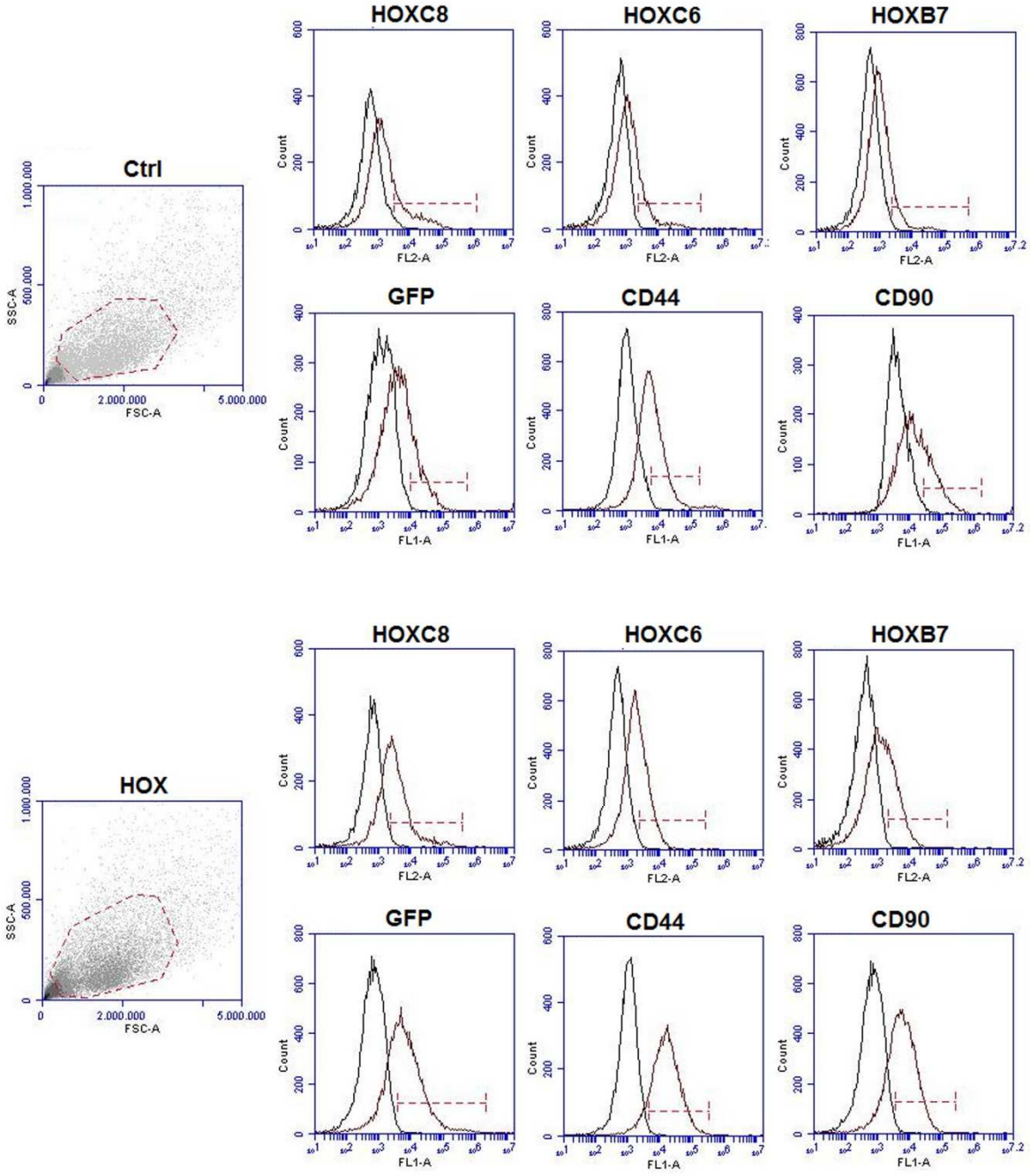

Supplemental Figure S3. Related to Figure 6.

Representative dot plots and histograms from the flow cytometry analysis as quantified and summarized in Figure 6B.

Single cell suspensions generated from freshly ex vivo isolated teratoma tissue pieces grown from implanted control- and *HOX*-transduced NEST-iPSCs were analyzed by FACS with indicated antibodies. 20.000-30.000 cells were analysed per sample. Representative blots are shown (biological replicates: n=8-10 for each epitope and group). Isotype controls are shown by the left peak. The red horizontal lines (red lines) depict the markers.

Figure S4

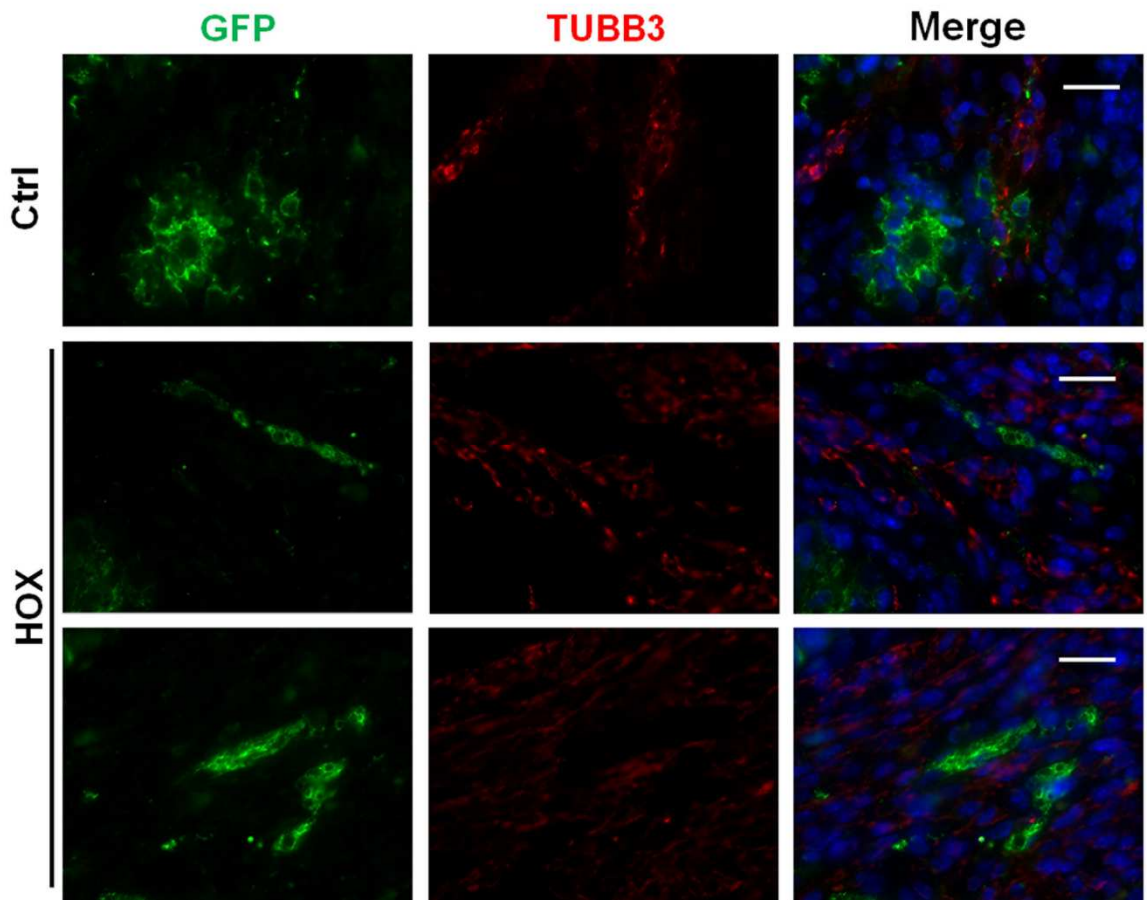

Supplemental Figure S4. Related to Figure 7.

Differentiated NEST-GFP(+) cells do not express neuronal beta-III tubulin.

Subcutaneously grown tumors were analysed by immunofluorescence and confocal microscopy. Sections were stained for GFP and (green) and beta-III tubulin (TUBB3) (red) Representative images from n=4 independent experiments are shown. Magnification 63x (scale bars 20µm).

2. Supplemental Tables

Table S1. Reprogramming efficiencies. Related to Figure 1.

Fibroblasts	**Seeded**	**Transduction efficiency in %**	**Clones isolated**	**Reprogramming efficiency in %**
Mouse 1	10.000	39	412	1.08
Mouse 2	10.000	18	269	1.49
Mouse 3	10.000	16	488	3.05

Table S2. Antibodies used in this study. Related to Figure 1-7.

Antibody, Clone (host)	Supplier	Cat#	Dilution
Nestin, H85 (rabbit)	Santa Cruz Biotech	sc-20978	1:200
GFP, 15 (mouse)	Santa Cruz Biotech	sc-101525	1:500
GFP, G10362 (rabbit)	Invitrogen	991639	1:500
HOXB7, 747C4a (mouse)	Santa Cruz Biotech	sc-81292	1:200
HOXB7, Z25 (rabbit)	Santa Cruz Biotech	sc-133670	1:200
HOXC6, B7 (mouse)	Santa Cruz Biotech	sc-376330	1:200
HOXC6 (rabbit)	Acris Antibodies	AP06660PU-N	1:200
HOXC8 (rabbit)	Bioss Inc.	bs-0394R	1:200
CD44, IM7 (rat)	Biolegend	103002	1:200
CD90, 3H1751 (rat)	Novus Biologicals	NB-200-528	1:200
CD73, TY/23 (rat)	BD Bioscience	550741	1:100
CD31, SZ31 (rat)	Dianova	DIA-310	1:200
Actin, AC74 (mouse)	Sigma-Aldrich	A2228	1:5000
Vimentin, EPR3776 (rabbit)	Abcam	ab92547	1:500
Catenin beta, E5 (mouse)	Santa Cruz Biotech	sc-7963	1:200
Alpha fetoprotein (rabbit)	Dako	A000829-2	1:200
Beta III tubulin (mouse)	Life Technologies	PA-1-46430	1:200
GFAP (rabbit)	Abcam	ab7260	1:200
PAX6 (rabbit)	Thermo Fischer Scientific	42-6600	1:100
Actin alpha sacromeric, 5C5 (mouse)	Sigma-Aldrich	A2172	1:200
OCT3/4, 40 (mouse)	BD Bioscience	611203	1:100
SSEA1, 480 (mouse)	Santa Cruz Biotech	sc-21702	1:100
SOX2, Btjce (rat)	eBioscience	14-9811-82	1:100
SOX2, D17 (goat)	Santa Cruz Biotech	sc-17319	1:200

Table S3. Oligonucleotides used for qRT-PCR. Related to Figure 1, 2 and 4.

Gene	sense/antisense	Primer sequence
Oct4	s	5'–CGC–CCG–CAT–ACG–AGT–TCT–3'
	as	5'–GCA–CCA–GGG–TCT–CCG–ATT–T–3'
Klf4	s	5'–CCA–GGA–GAA–CCC–CAA–GAT–GC–3'
	as	5'–GGG–TGC–CCT–GCT–GCG–AGT–A–3'
HOXB7	s	5'–CCG–AGA–GTA–ACT–TCC–GGA–TCT–A–3'
	as	5'–TCT–TGA–TCT–GTC–TTT–CGG–TGA–A–3'
HOXC6	s	5'–ATG–CTC–TCA–AAC–TGC–AGA–CAA–A–3'
	as	5'–CGA–GTT–AGG–TAG–CGG–TTG–AAG-T–3'
HOXC8	s	5'–AAG–GAC–AAG–GCC–ACT–TAA–ATC–A–3'
	as	5'–CCT–CCT–CTT–TCT–CCT–CTT–CCT–C–3'
GFP	s	5'–ACG–TAA–ACG–GCC–ACA–AGT–TC–3'
	as	5'–AAG–TCG–TGC–TGC–TTC–ATG–TG3–3'
Sca-1	s	5′-ACT-GTG-CCT-GCA-ACC-TTG-TCT-GAG-A-3′
	as	5′-GTC-CAG-GTG-CTG-CCT-CCA-TT-3′
c-Kit	s	5′-GCC-CTA-ATG-TCG-GAA-CTG-AA-3′
	as	5′-TTG-CGG-ATC-TCC-TCT-TGT-CT-3′
Nestin	s	5′-TCA-AGG-GGA-GGC-CAG-GAA-GGA-3′
	as	5′-CTG-CAG-CCC-CAC-TCA-AGC-CAT-C-3′
Adiponectin	s	5′-AGC-CGC-TTA-TGT-GTA-TCG-CT-3′
	as	5′-GAG-TCC-CGG-AAT-GTT-GCA-GT-3′
Osteocalcin	s	5′-GCA-ATA-AGG-TAG-TGA-ACA-GAC-TCC-3′
	as	5′-GTT-TGT-AGG-CGG-TCT-TCA-AGC-3′
Aggrecan	s	5′-CCC-TCG-GGC-AGA-AGA-AAG-AT-3′
	as	5′-CGC-TTC-TGT-AGC-CTG-TGC-TTG-3′

Specific primers were designed with the program Primer 3 (http://frodo.wi.mit.edu/cgi-bin/primer3/primer3_www.cgi) based on available NCBI nucleotide CDS sequences. Cross-reaction of primers was excluded by comparison of the sequence of interest with the NCBI database (Blast 2.2, U.S. National Centre for Biotechnology Information, Bethesda, MD) and all primers used in our study were intron-spanning. PCR products are 200-300 bp in size.

as

3. Supplemental Experimental Procedures

Tail-tip fibroblast isolation

An ~1 cm length of tail-tip from 8-week-old male nestin-GFP (NEST-GFP) transgenic donor mice was washed with 70% ethanol and PBS, the superficial dermis was peeled off, and the remaining tissue was cut into 1-mm pieces using a scalpel (1, 2). Five or six pieces were plated in one well of a 0.1% gelatin-coated six-well plate and cultured with 2 mL of Dulbecco's modified Eagle's medium (DMEM, high glucose) with 10% FBS, 1% Sodiumpyruvate and 50 units/mL penicillin/streptomycin (nTTF medium) for 5–7 days. Cells migrating out were trypsinized and expanded into T75 flasks (passage 1).

Reprogramming of mouse NEST-GFP tail-tip fibroblasts

We reprogrammed primary dermal tail tip fibroblasts from a transgenic mouse in which the gene encoding GFP is expressed under the regulatory control of the nestin promotor (NEST-GFP) (Klein et al., 2014). Transduction of fibroblasts was performed with a lentiviral vector co-expressing the four Yamanaka factor genes (*OCT4*, *KLF4*, *SOX2* and *MYC*) together with the coding sequence of the red fluorescent tdTomato protein (3). Expression plasmids encoding lentiviral gag-pol (pcDNA3.GP.CCC), HIV-rev (239_RSV_Rev) and the reprogramming cassette (pRRL.PPT.SF.OKSM.I.GFP.Pre) were transiently transfected into HEK293 cells together with pMDG_VSVG for pseudotyping (Stanurova et al., 2016). Culture supernatants were collected 24 and 48 hours post transfection. The produced virus was concentrated by ultracentrifugation of the supernatants at 27,000 x g, 1.5 h, 4 °C and titrated on HT1080 cells.

HOX gene expression vector and transduction

Generated NEST-GFP iPSCs were transduced using a lentiviral self-inactivating (SIN) vector (4, 5) co-expressing the coding sequences of *HOXB7*, *HOXC6* and *HOXC8* separated by *2A esterase* elements together with the gene encoding TURQUOISE2 (cyan) fluorescent protein (Figure 1C) (6).

Alkaline phosphatase staining

iPSC colonies were stained for alkaline phosphatase activity using the Alkaline Phosphatase Detection Kit from Millipore as recommended by the manufacturer. The staining reaction was stopped after 15 minutes by washing with PBS and cell colonies were evaluated by phase contrast microscopy.

Trilineage differentiation assay

Differentiation of cultivated MSCs into adipocytes, chondrocytes, and osteocytes was done using ready-to-use differentiation media from Lonza (hMSC Differentiation BulletKit–Adipogenic, PT-3004; –Chondrogenic, PT-3003; –Osteogenic, PT-3002) according to the manufactures instructions. Adipogenic differentiation was verified using Oil red staining, and osteogenic differentiation was verified using NBT/BCIP staining (Sigma) for alkaline phosphatase activity.

Cell proliferation assay

The number of living cells was determined upon staining of the cells with the vital dye trypan blue. For this, cells were harvested with Trypsin-EDTA, re-suspended in fresh medium, diluted with trypan blue, and counted at the indicated time points employing a Neubauer chamber.

RNA isolation and cDNA synthesis.

For RNA isolation the cells were lysed directly in the plastic Petri dishes as previously described and the RNA was isolated using RNeasy Mini Kit (Qiagen, Hilden, Germany) according to the manufacturer's instructions (Klein et al. 2013 and 2016a).

Flow cytometry

For FACS analysis of pluripotent cells, cells were treated with Trypsin/EDTA (Life Technologies) to generate a single-cell suspension, which was passed through a 40 µm cell strainer and counted. For FACS analysis of teratoma cells, freshly ex vivo isolated tissue pieces were mechanically minced and dissociated for 15-20 minutes at 37°C

in OptiMEM-I medium containing 0.2% type 2-collagenase (CLS2, ≥125 units per mg dry weight; Worthington, Lakewood, WA). Cells were washed twice in PBS/5% FCS and passed through a 40 µm cell strainer and counted. For each antibody staining, $1x10^5$ cells were used in a volume of 100-200 µl FACS buffer (10% FBS in PBS). Antibodies were used in a 1:100 dilution and incubated with the cell suspension for 20 min at 4 °C. For staining of nuclear proteins, cells were fixed prior staining using 4 % paraformaldehyde for 15 min at room temperature and permeabilized by incubation in 0.1 % (v v) Triton X-100 for 5 min at room temperature prior antibody staining. After addition of 1 ml FACS buffer and centrifugation (700 x g, 5 min), cells were resuspended in 200 µl FACS buffer and analyzed on a FACS Aria (Becton Dickinson) using the FACSDiva software (Becton Dickinson). Isotype controls were applied for every antibody. Data analysis was done using Kaluza® software (Beckman Coulter). Antibodies are listed in Table S2.

Real-time RT-PCR analysis.

Analysis was carried out using the oligonucleotide primers listed in Table S3. The PCR program consisted of initial denaturation at 95°C for 30 s, annealing at 58°C for 40 s and extension at 72°C for 30 s for 25-30 cycles. Specificity of all PCR reactions was tested by parallel reactions using water instead of cDNA. Real-time PCR analysis was performed using SYBR®Green PCR Master Mix (Applied Biosystems, Darmstadt, Germany) and standard conditions. The experiments were performed on ABI PRISM® 7000 sequence detection system (Applied Biosystems). Expression levels of analysed genes were normalized to the reference gene β-actin mRNA expression (relative quantification). Mean values ± SEM from at least three independent samples per group and gene were quantified, measured in duplicates each

Western blot

Whole cell lysates were generated by scraping cells into ice-cold RIPA-P buffer (150 mmol/L NaCl, 1% NP40, 0.5% sodium-desoxycholate, 0.1% sodium-dodecylsulfate, 50 mmol/L Tris/HCL pH 8, 10 mmol/L NaF, 1 mmol/L Na_3OV_4), supplemented with a complete Protease-Inhibitor-Cocktail (Roche) and performing 2-3 freeze-thaw cycles. Protein samples (50–100 µg total protein) were subjected to SDS-PAGE electrophoresis and Western blots were done as previously described using HOXB7, HOXC6, HOXC8, GFP and NEST (all 1/200) or β-Actin (1/5000) antibodies (Klein et al. 2013 and 2014). For quantification, blots were analyzed by densitometry and the respective signal was related to the reference protein beta-actin.

4. Supplemental References

1. Yamaguchi M. Analysis of neurogenesis using transgenic mice expressing GFP with NESTin gene regulatory regions. Chemical senses. 2005;30 Suppl 1:i117-8.
2. Yamaguchi M, Saito H, Suzuki M, Mori K. Visualization of neurogenesis in the central nervous system using NESTin promoter-GFP transgenic mice. Neuroreport. 2000;11(9):1991-6.
3. Takahashi K, Yamanaka S. Induction of pluripotent stem cells from mouse embryonic and adult fibroblast cultures by defined factors. Cell. 2006;126(4):663-76.
4. Schambach A, Bohne J, Chandra S, Will E, Margison GP, Williams DA, et al. Equal potency of gammaretroviral and lentiviral SIN vectors for expression of O6-methylguanine-DNA methyltransferase in hematopoietic cells. Molecular therapy : the journal of the American Society of Gene Therapy. 2006;13(2):391-400.
5. Voelkel C, Galla M, Maetzig T, Warlich E, Kuehle J, Zychlinski D, et al. Protein transduction from retroviral Gag precursors. Proceedings of the National Academy of Sciences of the United States of America. 2010;107(17):7805-10.
6. Goedhart J, von Stetten D, Noirclerc-Savoye M, Lelimousin M, Joosen L, Hink MA, et al. Structure-guided evolution of cyan fluorescent proteins towards a quantum yield of 93%. Nature communications. 2012;3:751.